Sensory nerve regulates progenitor cells via FGF-SHH axis in tooth root morphogenesis

Fei Pei[1,2], Li Ma[1], Tingwei Guo[1], Mingyi Zhang[1], Junjun Jing[1], Quan Wen[1], Jifan Feng[1], Jie Lei[1], Jinzhi He[1], Eva Janečková[1], Thach-Vu Ho[1], Jian-Fu Chen[1] and Yang Chai[1]*

1. Center for Craniofacial Molecular Biology, University of Southern California, 2250 Alcazar Street, CSA 103, Los Angeles, CA 90033, USA

2. The State Key Laboratory Breeding Base of Basic Science of Stomatology (Hubei-MOST) & Key Laboratory of Oral Biomedicine Ministry of Education, School and Hospital of Stomatology, Wuhan University, Wuhan 430079, China

Corresponding author
Yang Chai, DDS, PhD
University Professor
George and MaryLou Boone Chair in Craniofacial Biology
Center for Craniofacial Molecular Biology
Ostrow School of Dentistry
University of Southern California
ychai@usc.edu

Key words: nerve, stem/progenitor cells, FGF signaling, organ morphogenesis, Hh signaling

Abstract

Nerves play important roles in organ development and tissue homeostasis. Stem/progenitor cells differentiate into different cell lineages responsible for building the craniofacial organs. The mechanism by which nerves regulate stem/progenitor cell behavior in organ morphogenesis has not yet been comprehensively explored. Here, we use tooth root development as a model to investigate how sensory nerves regulate organogenesis. We show that sensory nerve fibers are enriched in the dental papilla at the initiation of tooth root development. Through scRNAseq analysis of the trigeminal ganglion and developing molar, we reveal several signaling pathways that connect the sensory nerve with the developing molar, of which FGF signaling appears to be one of the important regulators. *Fgfr2* is expressed in the progenitor cells during tooth root development. Loss of FGF signaling leads to shortened roots with compromised proliferation and differentiation of progenitor cells. Furthermore, Hh signaling is impaired in *Gli1-Cre^{ER};Fgfr2$^{fl/fl}$* mice. Modulation of Hh signaling rescues the tooth root defects in these mice. Collectively, our findings elucidate the nerve-progenitor crosstalk and reveal the molecular mechanism of the FGF-SHH signaling cascade during tooth root morphogenesis.

Introduction

Nerves are crucial in tissue development, homeostasis and regeneration. For example, the nervous system plays important roles during the development of craniofacial tissues such as the salivary glands, teeth, and calvarial bones(1). Nerves directly regulate the morphogenesis of salivary glands by releasing vasoactive intestinal peptide (VIP), and depletion of nerves leads to disordered tubulogenesis of salivary glands(2). Sensory nerves modulate mesenchymal progenitor cells during calvarial bone development(3). Moebius syndrome, characterized by deficient innervation of the abducens (VI) and facial (VII) nerves, results in craniofacial malformations such as cleft palate and abnormal teeth(4, 5). Inherited peripheral nervous disorders, such as mutation of the neurotrophic tyrosine kinase receptor 1 gene (*NTRK1*), can lead to craniofacial defects including cleft palate, nasal malformation and tooth agenesis(1, 6). Nerves are also involved in homeostasis of tissues such as bone, hair follicles and rodent incisors. In craniofacial tissues, sensory nerves are crucial for mesenchymal stem cell maintenance and tissue homeostasis(7, 8). Sensory nerves also participate in the repair and regeneration of calvarial and mandibular bone(9, 10). These converging lines of evidence demonstrate that nerves are essential for craniofacial tissue morphogenesis, homeostasis and repair.

Stem and progenitor cells play important roles in development and organgenesis, and can self-renew and differentiate into multiple cell lineages. Stem cells differentiate in their specific tissue niches, which are complex environments regulated by a signaling pathway network(11). During development, stem cells undergo concerted and controlled clonal proliferation(12). The multipotential stem and progenitor cells in craniofacial tissues are important for the development of craniofacial organs through their carefully coordinated

migration, proliferation, and differentiation(13). Nerves have been found to regulate the fate of stem/progenitor cells in development and tissue homeostasis. Recently, interest has grown in how nerves regulate stem/progenitor cell behavior and what kinds of signals/factors are secreted from nerves in support of these processes.

Currently, factors belonging to the Netrin and Semaphorin families including SEMA3A, SEMA3C, NTN1, and NTN4 are known to play important roles in development and organ morphogenesis(14). During salivary gland morphogenesis, nerve-derived NRG1 regulates progenitors to mediate crosstalk between the nerve and the epithelium, influencing acinar specification(15). Sensory nerve-derived FSTL1 is known to modulate mesenchymal progenitor cells during the development of calvarial bone(3). Sensory nerves secrete SHH and FGF1 to maintain mesenchymal stem cells in the mouse incisor and maintain mesenchymal tissue homeostasis in this continuously growing organ(7, 8).

Tooth root development is an ideal model for studying organ morphogenesis and investigating the regulatory mechanism of the fate decision of cranial neural crest (CNC)-derived progenitor cells. This developmental process depends upon the appropriate proliferation and differentiation of stem and progenitor cells(16, 17). CNC-derived mesenchymal cells involved in tooth root development include dental papilla and dental follicle cells, which contribute mainly to the pulp and periodontal tissues(18, 19). *Gli1*$^{+}$ cells are multipotent mesenchymal stem cells (MSCs) that support mouse tooth root growth(16). The tooth is a highly innervated organ, with innervation beginning in embryonic stages and continuing throughout life. However, the mechanism by which sensory nerves regulate the fate of progenitor cells to modulate tooth root morphogenesis is still unclear.

In this study, we used the murine molar tooth roots as a model to study the role of sensory nerves in organ morphogenesis, and the mechanism by which they exert this role. We detected the spatial distribution of nerves using whole-mount staining, which showed that nerves are enriched in the apical papilla and reach the coronal papilla in the molar. Using scRNAseq analysis of the trigeminal ganglion and molar, we detected several signaling pathways that connect the sensory nerve with the developing molar, of which FGF signaling appears to be one of the most important regulators for root development. We discovered that *Fgfr2* is expressed in progenitor cells receiving sensory nerve-derived FGF signaling. The loss of *Fgfr2* in *Gli1*$^{+}$ progenitors led to shortened roots, accompanied by decreased cell proliferation, impaired dentin formation, and defects in periodontal ligament differentiation. The level of SHH, a Hh signaling ligand, decreased after loss of FGF signaling, which further showed that Hh signaling is compromised. By modulating the activity of Hh signaling, we were able to partially rescue the cellular defects and shortened roots in *Gli1-Cre*^{ER}*;Fgfr2*$^{fl/fl}$ mice. Our study illustrates how the sensory nerve controls this FGF-SHH signaling cascade to regulate progenitor cell fate during tooth root morphogenesis.

Results

Sensory nerve regulates papilla and follicle cells through FGF signaling upon the initiation of tooth root development

The majority of nerve fibers in the tooth are sensory, and the axons in the dental pulp belong to sensory neurons from the trigeminal ganglion(7, 8). To explore the distribution of nerves in the molar in the initial stage of tooth root development, whole-mount neurofilament staining of first molars was performed. 3D images of nerves in the molar (Movie 1) clearly showed enrichment of nerves in the apical papilla, which pass through the middle papilla to reach the cusp region of the developing molar at postnatal day (PN)3.5 (Fig. 1A-D). This suggested that nerves may play a crucial role in regulating tooth root development. To investigate signals derived from the sensory nerve at this stage, we performed scRNAseq of the trigeminal ganglion at PN3.5 (Fig. 1E). Different clusters were identified, including sensory neurons, neural progenitor cells, glial cells and others. Clusters of sensory neurons were identified with markers *Tubb3*, *Rbfox3, Calca,* and *Mfap4*. Clusters of neural progenitors were identified with the marker *Sox2*. Clusters of Schwann cells were identified with the markers *Plp1* and *Mag*. Clusters of glial cells were identified with the markers *Plp1*, *Mag*, *Mpz* and *Gfap* (Fig. S1). The rest of the clusters were identified as immune cells (*Lyd6*), microglia (*Ctss*), cycling cells (*Top2a*), arterial smooth muscle cells (*Acta2*), endothelial cells (*Cdh5*) and meningeal cells (*Dcn*) (Fig. S1).

To further study the interaction between the sensory nerves and cells in the developing molar, we integrated the sensory neuron clusters from the trigeminal ganglion with cell clusters from scRNAseq data of the molar at PN3.5 performed for our previous study(19). We analyzed the significant signals from the sensory nerve after importing the integrated

Seurat object into CellChat. It showed that ANGPTL, FGF, NCAM, HH, PDGF and THBS could be derived from the sensory nerve and regulate cells in the molar (Fig. 1F). Among the signals that were identified, FGF signaling was the most significant one that derived mainly from the sensory nerve, whereas the other signals were also secreted from epithelial and mesenchymal cells in the developing molar (Fig. 1F-G). Moreover, FGF signaling from the nerve mainly regulated mesenchymal cells including dental papilla and follicle cells (Fig. 1G). We found that *Fgf1* is the ligand secreted from sensory neurons based on scRNA of the trigeminal ganglion and verified *in vivo* that *Fgf1* is expressed in sensory neurons in the trigeminal ganglion (Fig. 1H-J).

When we examined transcripts of *Fgf1* in the mouse molar, we found that little *Fgf1* was expressed in the developing molar in our scRNA-seq data and *in vivo* staining (Fig. 1K-M). However, the expression of FGF1 protein was detected in the mesenchymal tissue of the molar, mainly in the apical and coronal papilla, and its distribution was similar to that of the sensory nerve (Fig. 1N-P). These results suggested that the sensory nerve secretes FGF1 at the initiation of mouse molar root development, and nerve-derived FGF signaling plays an important role in regulating tooth root morphogenesis. Since various FGF ligands are present in the early stages of tooth development during embryogenesis, we also detected canonical FGF ligands in the molar during its postnatal development. Unlike in embryonic development, only *Fgf3* expression and some small amounts of *Fgf8* and *Fgf10* were detected in scRNA-seq data from the postnatal molar (Fig. S2A). The expression of *Fgf3* was limited to the apical papilla, and scattered and weak expression of *Fgf10* and *Fgf8* was detected in the apical papilla and pre-odontoblasts, respectively (Fig. S2B-G). Previous studies also found that *Fgf10* almost disappears from the tooth

postnatally(20), which is consistent with our results. To investigate the local FGF signaling in the molar, we analyzed the signaling pathway interaction among different cell clusters in the molar. FGF signaling was not among the top 20 signaling pathways detected, whereas local ncWNT, BMP, WNT, HH and IGF were all significant signals during postnatal molar development (Fig. S2H). All these data suggested that nerve-derived FGF signaling is crucial at the initial stage of tooth root development.

Sensory nerve modulates *Gli1*$^{+}$ progenitor cells through FGF signaling

Previous study has shown that the dental papilla can give rise to dental pulp cells and odontoblasts, while the dental follicle can give rise to alveolar bone, periodontal ligament, and cementum(19). These processes coordinately support tooth root morphogenesis. To better evaluate the cell domains and associated gene expression patterns, we performed an unbiased comprehensive gene expression study by analyzing our PN3.5 scRNAseq data of the first molar(19), which included dental papilla, dental follicle, cycling cells, epithelial cells, endothelial cells, glial cells and immune cells (Fig. 2A). Clusters 0, 1 and 2 were identified as dental papilla cells with markers *Aox3*, *Nnat* and *Enpp6*. Clusters 4 and 6 were identified as dental follicle cells with markers *Bmp3* and *Smoc2*. Clusters 3, 7, 10 and 15 were identified as epithelial cells with marker *Krt14* (Fig. S3A). The rest of the clusters were identified using established markers as immune cells (5, 12, 14 and 16), endothelial cells (8), glial cells (11), cycling cells (9) and odontoblasts (13) (Fig. S3A).

Since progenitor cells in the molar are crucial for tooth root development, we investigated how sensory nerve-derived FGF signaling regulates progenitor cells to modulate tooth root morphogenesis. FGF signaling is activated by binding with different FGF receptors. We evaluated FGF receptors during tooth root development using our scRNAseq data. A

feature plot showed that *Fgfr2* was expressed in the dental follicle, papilla cells, and epithelial cells, which are important for tooth root development (Fig. S3B). *Fgfr1* was widely expressed in follicle and papilla cells as well as epithelial cells, especially strongly in the coronal papilla, and *Fgfr3* was detected in the coronal and middle papilla (Fig. S3B). Moreover, *Fgfr2* was colocalized with *Gli1*$^{+}$ cells in the dental follicle and papilla as well as apical epithelial cells (Fig 2B-D), which are progenitor cells during tooth root development. We also examined the expression of *Fgfr2* during tooth root development. It was expressed in the apical dental papilla, the dental follicle, and the apical epithelium at PN3.5 and PN7.5 (Fig. 2E-F, Fig. S4A-B). Later in tooth root development, at PN13.5, *Fgfr2* was detected in the periodontal region and the apical dental mesenchymal cells (Fig 2G-H). Then a more restricted pattern of *Fgfr2* expression was present in the periodontal region at PN21.5 (Fig 2I-J). These results suggested that sensory nerve-derived FGF signaling may modulate *Gli1*$^{+}$ progenitor cells through *Fgfr2* during tooth root development.

Ablation of *Fgfr2* in *Gli1*$^{+}$ progenitor cells results in shortened roots with compromised cell proliferation and differentiation

To test our hyphothesis that sensory nerve-derived FGF signaling may modulate *Gli1*$^{+}$ progenitor cells through *Fgfr2*, we deleted *Fgfr2* from the *Gli1*$^{+}$ progenitors by generating *Gli1-Cre*^{ER}*;Fgfr2*$^{fl/fl}$ mice and confirmed that *Fgfr2* expression was efficiently reduced in these mice (Fig. S4A-D). Based on histological analysis, a tooth root defect was detectable at PN13.5 and onwards. Compared to the root elongation observed in control mice at PN13.5, this elongation process was delayed in *Gli1-Cre*^{ER}*;Fgfr2*$^{fl/fl}$ mice and accompanied by abnormal odontoblast alignment (Fig. S4E-I). Consistent with the

morphological changes, odontoblast differentiation indicated by *Dspp* expression was impaired in the *Gli1-Cre^{ER};Fgfr2$^{fl/fl}$* mice (Fig. S4J-N). Periodontal ligament differentiation was also defective, as indicated by periostin expression in the *Gli1-Cre^{ER};Fgfr2$^{fl/fl}$* mice (Fig. S4O-S). By PN21.5, the roots were still shorter in the *Gli1-Cre^{ER};Fgfr2$^{fl/fl}$* mice than in controls, as revealed through CT and histological analysis (Fig 3A-E), with impaired odontoblast and periodontal ligament differentiation in both the lateral and the furcation regions of the tooth (Fig. 3H-M).

Since *Fgfr2* is also expressed in the epithelium, we wanted to test whether loss of *Fgfr2* in epithelial progenitor cells may adversely affect mesenchymal progenitors during tooth root development by generating *K14rtTA;tetO-Cre;Fgfr2$^{fl/fl}$* mice. *Fgfr2* was efficiently deleted in the epithelium while it could still be detected in dental follicle and papilla cells at PN7.5 (Fig. S5A-D). There was no obvious difference in root length between the control and *K14rtTA;tetO-Cre;Fgfr2$^{fl/fl}$* mice (Fig. S5E-I). Odontoblast and periodontal ligament differentiation were not affected in *K14rtTA;tetO-Cre;Fgfr2$^{fl/fl}$* mice (Fig. S5J-O). This suggested that the root length defect was not caused by the loss of FGF signaling in the dental epithelium in *Gli1-Cre^{ER};Fgfr2$^{fl/fl}$* mice. These results corroborated our CellChat result that nerve-derived FGF signaling predominantly regulates dental papilla and follicle cells. All these results illustrated that *Fgfr2* in the dental mesenchymal progenitors plays an important role in regulating root development and that its loss leads to shortened roots, as well as defects in odontoblast and periodontal ligament differentiation.

To explore the root defects in *Gli1-Cre^{ER};Fgfr2$^{fl/fl}$* mice and determine the underlying mechanism, we investigated the cell fate of *Gli1^{+}* progenitors during the course of root development. We found that the proliferation rate indicated by Ki67 staining was

significantly decreased in the apical epithelium and mesenchyme surrounding Hertwig's epithelial root sheath (HERS) in *Gli1-Cre^{ER};Fgfr2$^{fl/fl}$* mice (Fig. 3N-R). To investigate where proliferation was primarily affected, we tested it at PN5.5 and found that proliferation was decreased in the mesenchyme, but was not significantly changed in the epithelium at this stage (Fig. S6A-F). This result suggested that proliferation primarily decreased in the mesenchyme, which led to decreased proliferation in the epithelium after *Fgfr2* was deleted in *Gli1*$^{+}$ progenitor cells. Then, analysis of apoptosis with TUNEL staining showed sparse TUNEL^{+} apoptotic cells in the *Gli1-Cre^{ER};Fgfr2$^{fl/fl}$* mice with no significant difference from the control group (Fig. S6G-K). These results suggested that loss of FGF signaling in *Gli1*$^{+}$ progenitor cells is responsible for the tooth root defects in *Gli1-Cre^{ER};Fgfr2$^{fl/fl}$* mice, including shortened roots with compromised root progenitor cell proliferation and differentiation.

Loss of FGF signaling leads to impaired Hh signaling in root progenitor cells

To investigate the mechanism by which nerve-derived FGF signaling regulates tooth root development, we performed RNA sequencing of the apical region of control and *Gli1-Cre^{ER};Fgfr2$^{fl/fl}$* mouse first molars, including the dental mesenchyme and epithelium, at PN7.5. The heatmap showed well-separated gene expression profiles distinguishing the two groups (Fig. 4A). A total of 739 differentially expressed genes were found (>1.5-fold, $p < 0.05$), of which 413 were upregulated and 326 were downregulated in the *Fgfr2* mutant relative to the control (Fig. 4B). Gene Ontology (GO) analysis showed that FGF signaling and Hh signaling were involved (Fig. 4C), which suggested that Hh signaling might be disturbed in the developing root region in *Gli1-Cre^{ER};Fgfr2$^{fl/fl}$* mice. Moreover, *Gli1*, a transcript downstream of Hh signaling, decreased significantly in the *Gli1-Cre^{ER};Fgfr2$^{fl/fl}$*

mice (Fig. S7). We verified these results *in vivo* to see the change in Hh signaling after *Fgfr2* was deleted in the *Gli1*$^{+}$ progenitor cells. *Ptch1*, the receptor of Hh ligand, was expressed in the apical mesenchyme adjacent to the dental epithelium and the follicle cells in the control, but its expression was compromised in the apical mesenchymal and epithelial cells in *Gli1-Cre*^{ER}*;Fgfr2*$^{fl/fl}$ mice (Fig. 4D-H). *Gli1* showed a similar expression pattern, which was also decreased significantly in both epithelial and mesenchymal cells in *Gli1-Cre*^{ER}*;Fgfr2*$^{fl/fl}$ mice at PN7.5 (Fig. 4I-M). In summary, our results indicated that the loss of FGF signaling in *Gli1*$^{+}$ progenitor cells leads to impaired Hh signaling during tooth root development.

Impaired SHH leads to decreased Hh signaling in *Gli1-Cre*^{ER}*;Fgfr2*$^{fl/fl}$ mice

To investigate how FGF signaling regulates Hh signaling, we examined ligands of Hh signaling in the first molar. A feature plot showed that *Shh* was expressed in epithelial cells, whereas neither *Dhh* nor *Ihh* expression was detectable in the molar (Fig. 5A-B). *Shh* was widely expressed in the epithelium of the molar, especially in apical epithelial cells at PN3.5, and decreased at PN7.5 (Fig. 5C, G-H). *Dhh* and *Ihh* could barely be detected in the molar at PN3.5 (Fig. 5D-E). Since both *Ptch1* and *Gli1*, which are Shh target genes, were downregulated in both dental epithelium and mesenchyme in *Gli1-Cre*^{ER}*;Fgfr2*$^{fl/fl}$ mice, we analyzed *Shh* expression in our RNA-seq results and determined that *Shh* was downregulated in *Gli1-Cre*^{ER}*;Fgfr2*$^{fl/fl}$ mice (Fig. 5F). We verified *in vivo* that the transcript of *Shh* and protein level were decreased in *Fgfr2* mutant mice (Fig. 5G-O). These results demonstrated that impaired FGF signaling led to decreased SHH, which caused downregulation of Hh signaling during tooth root development.

Restoration of Hh signaling partially rescues short roots in *Gli1-Cre*^{ER}*;Fgfr2*$^{fl/fl}$ mice

To test whether compromised Hh signaling is responsible for causing the root development defect in *Gli1-Cre^{ER};Fgfr2$^{fl/fl}$* mice, we upregulated Hh signaling in dental root progenitor cells by generating *Gli1-Cre^{ER};Fgfr2$^{fl/fl}$;SmoM2$^{fl/+}$* mice. At PN21.5, the shortened root length was partially rescued with the upregulation of Hh signaling in the *Gli1-Cre^{ER};Fgfr2$^{fl/fl}$;SmoM2$^{fl/+}$* mice in comparison to *Gli1-Cre^{ER};Fgfr2$^{fl/fl}$* mice (Fig. 6A-J). Moreover, the odontoblast and periodontal ligament differentiation defects were partially rescued (Fig. 6K-O). We further examined cellular changes after Hh signaling was upregulated in the *Gli1-Cre^{ER};Fgfr2$^{fl/fl}$;SmoM2$^{fl/+}$* mice. We found that proliferation was restored to a level comparable to controls in *Gli1-Cre^{ER};Fgfr2$^{fl/fl}$;SmoM2$^{fl/+}$* mice at PN7.5 (Fig. 6P-V). These results suggested that the FGF-Hh signaling cascade plays a crucial role in regulating tooth root morphogenesis, as well as modulating progenitor cell proliferation and differentiation.

Discussion

Nerves are known to contribute to craniofacial development. However, it is still largely unknown how sensory nerves function in regulating the fate of progenitors during organogenesis. Tooth root development is a good model through which we can investigate the dynamic processes of progenitor cell fate regulation during organogenesis (19). Here, we investigated nerve-progenitor cell interaction in this context. We found that sensory nerves regulate progenitor cells through FGF signaling. Briefly, nerve-derived FGF1 regulates proliferation and differentiation of progenitors through *Fgfr2*, loss of which in *Gli1*$^{+}$ progenitor cells leads to tooth root defects. Furthermore, SHH is downregulated following the loss of FGF signaling, which leads to decreased Hh signaling and adversely affects FGF signaling specificity in regulating tooth root development (see Fig. 7 for summary).

Mammalian teeth are densely innervated by sensory neurons from the trigeminal ganglion. The outgrowing axons of the trigeminal ganglion can be observed at E9.5, enter the mandibular process around E10, and subsequently participate in tooth germ initiation during later embryonic stages(21). This suggests close interaction between sensory nerves and the developing tooth germs. We showed the spatial distribution and specific enrichment of nerves in the dental papilla at the initiation of tooth root development. Moreover, we found that FGF is the most significant signaling originating from these sensory nerves. Our previous study showed that sensory nerve-derived FGF signaling is important for adult stem cell maintenance and tissue homeostasis(8). Here, we revealed that sensory nerve-derived FGF signaling also regulates progenitor cells to modulate organ morphogenesis. The particular FGF ligand secreted from the sensory nerve is

FGF1, and it activates different receptors to play specific roles in different tissues. Moreover, nerve-derived FGF signaling utilizes different downstream molecules to control the fate of stem/progenitor cells. Although FGF1 from the sensory neurons of the trigeminal ganglion is present at both PN3.5 and later in adult stages, the amount of FGF1 is greater in adult sensory neurons. Such signaling molecules may exhibit spatiotemporal changes depending on the context and the specific role in the tissue. In addition to FGF signaling, other pathways such as HH, PDGF, EGF and THBS were found to be involved in nerve-molar interaction in this study, and merit further study in the future.

Since FGF signaling plays an important role in embryonic tooth development, it makes sense that we have also identified some gene expression representing local FGF ligands, such as *Fgf3*, *Fgf8* and *Fgf10*, in the developing molar. For example, *Fgf10* expression is present in the mesenchyme during early stages of tooth formation but is no longer present after the initiation of root development, which suggests that *Fgf10* may regulate the switch between crown and root formation(20, 22). Consistent with our study, we found *Fgf3* expression in the apical papilla, and *Fgf8* and *Fgf10* were expressed at lower levels. A previous study showed that *Fgf3*+ cells can give rise to dental pulp cells and odontoblasts(19). Despite the presence of these FGF ligands in the developing molar, we have yet to gain a comprehensive understanding of FGF signaling mechanism in regulating molar root development. Importantly, our study suggests that sensory nerve-derived FGF signaling is crucial for the progenitor cell fate decision during tooth root development.

Signaling pathways can activate transcription factors which in turn affect other signaling pathways, thus forming intricate signaling networks (17). A recent study showed that the

mTOR/autophagy axis is downstream of nerve-derived FGF signaling in the maintenance of adult stem cells(8). Crosstalk between FGF and Hh signaling controls organ branching and morphogenesis in developmental contexts such as the kidney(23), lung(24), and limb(25). Previous study showed that FGF promotes *Shh* expression by increasing *Etv* expression, and that this FGF-ETV-SHH feedback loop participates in the lung branching rhythm(24). In our study, we have shown that FGF/SHH signaling modulates tooth root morphogenesis. Our results show that the decreased *Shh* expression in the dental epithelium might be the indirect effect following the loss of *Fgfr2* in Gli1+ progenitors. Since epithelium and mesenchyme interacts during tooth root development, the decreased SHH in the epithelium has adverse effects on mesenchymal cells. This suggests FGFR2-dependent mesenchymal proliferation and differentiation have a direct effect on tooth root morphogenesis. In addition, the reduced Shh signaling in the dental epithelium also has an adverse effect on root formation. It is clear that FGF and Hh signaling co-occur during the morphogenesis of multiple organs and tissues. The Hh signaling pathway governs multiple genes that regulate cell proliferation and differentiation(26, 27). Previous study has revealed that either inhibition or overactivation of Hh signaling results in shortened tooth roots with decreased cell proliferation(28), which suggests proper level of Hh signaling is essential to establish tooth roots. Our study showed that decreased Hh signaling led to decreased cell proliferation and differentiation during root development, and re-activation of Hh signaling partially restored the tooth root defect seen after loss of FGFR2. It suggests the interaction between FGF and Hh signaling in mesenchyme and epithelium is important for tooth root development. During craniofacial development, loss or overactivation of Hh signaling in neural crest cells can

cause skeletal abnormalities(29). These findings suggest that proper Hh activity is crucial for cell proliferation and differentiation, and therefore organ morphogenesis. Sensory nerve-derived FGF signaling determines the fate of progenitor cells through an FGF-SHH signaling cascade during tooth root development.

In summary, we have revealed that sensory nerves regulate progenitor cell fate through FGF1-FGFR2 interaction and are involved in the regulation of tooth root morphogenesis via the FGF-SHH signaling axis. This finding improves our understanding of the mechanism by which sensory nerves participate in guiding organ morphogenesis and offers crucial information on how to control progenitor cells in tissue regeneration.

Materials and Methods

Animals

Gli1-LacZ (JAX# 008211)(30), *Gli1-Cre^{ER}* (JAX#007913)(31), *Fgfr2$^{fl/fl}$* (from Dr. Philippe Soriano)(32), *K14-rtTA* (JAX# 007678)(33), *Teto-Cre* (JAX# 006234)(34), and *SmoM2$^{fl/fl(29)}$* mouse lines were used in this study. All mice were housed in pathogen-free conditions. All animal studies were approved by the Institutional Animal Care and Use Committee (IACUC) at the University of Southern California (USC).

Tamoxifen and doxycycline administration

Tamoxifen (Sigma, T5648) was dissolved in corn oil (Sigma, C8267) at 20 mg/ml. *Fgfr2$^{fl/fl}$*, *Gli1-Cre^{ER};Fgfr2$^{fl/fl}$* and *Gli1-Cre^{ER};Fgfr2$^{fl/fl}$;SmoM2$^{fl/+}$* mice were injected intraperitoneally at a dosage of 1.5 mg/10 g body weight at PN3.5. Dams giving birth to *K14rtTA;tetO-Cre;Fgfr2$^{fl/fl}$* mice were fed with a doxycycline rodent diet (Envigo, TD.08541) every day beginning when the suckling pups were at PN3.5. A dosage of 50 mg/mL doxycycline (Sigma-Aldrich; D9891) was injected into the pups intraperitoneally at PN3.5.

Tissue clearing and staining

Mandibles were collected from wild-type mice at PN3.5 and fixed with 4% paraformaldehyde. The molars were dissected and transparentized with tissue clearing reagent (TCI, T3741) following the manufacturer's protocol. The molars were incubated with neurofilament antibody (1:100, Abcam, ab4680) at 4°C overnight, and Alexa-conjugated secondary antibody (1:200, Invitrogen) was used to detect signals. Images were captured with a confocal microscope (Leica, Stellaris confocal).

Single-cell isolation from trigeminal ganglion and single-cell RNA-sequencing (scRNA-Seq)

Mice at PN3.5 were euthanized by CO_2 inhalation and decapitation. Bilateral trigeminal ganglia (TG) were carefully dissected. Briefly, the skull was removed and the brain was carefully flipped to expose the TG. The three branches of the TG were severed and carefully dissected from the surrounding bone structure under a microscope. The TG was then chopped into small pieces in a sterile tube and dissociated with a papain dissociation system (Worthington, Lakewood, NJ, USA) according to the manufacturer's instructions. The mixture was incubated on a thermomixer (Eppendorf) at a 37°C for 40 min. The cloudy cell suspension was carefully removed, placed in a sterile tube and centrifuged at 300g for 5 minutes. The supernatant was discarded, and cell pellets were resuspended in a DNase/papain-inhibitor solution. Discontinuous density gradient centrifugation was performed (70 g for 6 min), and then the cell pellets were resuspended in medium to obtain a single-cell suspension. Cells were loaded into a 10X Chromium system using a Single Cell 3' Library Kit v3.1 (PN-1000269, 10X Genomics). Sequencing was performed on the Illumina Novaseq System. Raw read counts were analyzed using the Seurat 4.0 R package.

Single-cell RNA analysis

ScRNAseq data of mouse molar and trigeminal ganglion at PN3.5(19) were analyzed using the Seurat 4.0 R package(35). Cells with low gene expression and poor-quality cells were removed. Normalization, cell cycle regression, and RunPCA were performed. Visualization of the clusters was performed with RunUMAP. Published markers were used to identify the different cell populations in the mouse molar.

Integration and interaction analysis

scRNA-Seq data from the trigeminal ganglion and the molar were combined with Seurat and integration analysis was performed. RunPCA and RunUMAP were performed for further analysis.

CellChat(36) was used to explore the ligand-receptor interactions between trigeminal ganglion and molar. We imported the Seurat object into CellChat and used the following preprocessing functions with standard parameters to analyze the potential cell-cell communication network: identifyOverExpressedGenes, identifyOverExpressedInteractions and projectData. The core functions computeCommunProb, computeCommunProbPathway and aggregateNet were run to infer the communication network and signaling pathway, again with standard parameters. NetVisual_circle, netAnalysis_signalingRole_heatmap, and netAnalysis_signalingRole_network were used to analyze the signaling senders and receivers.

MicroCT analysis

Mandibles were collected from mice at PN21.5 and were fixed with 4% paraformaldehyde. MicroCT analysis was performed using a Skyscan 1174v1.2 (Bruker Corporation, USA) at 50 kVp, 800 μA and a resolution of 16.7 mm. Visualization and three-dimensional reconstruction were performed using Avizo/Amira 9.5.0 (Visualization Sciences Group, France).

In situ hybridization

Cryosections were stained according to the manufacturer's instructions using RNAscope Multiplex Fluorescent v2 kit (Advanced Cell Diagnostics, 323100). All probes used in this study were synthesized by Advanced Cell Diagnostics: Probe-Mm-*Fgf1* (466661), Probe-Mm-*Fgf3* (503101), Probe-Mm-*Fgf8* (313411), Probe-Mm-*Fgf10* (446371), Probe-Mm-*Fgfr2* (443501), Probe-Mm-*Dspp* (448301), Probe-Mm-*Ptch1* (402811), Probe-Mm-*Ptch1*-C2 (402811-C2), and Probe-Mm-*Gli1* (311001).

Histological analysis

Mouse mandibles were dissected and fixed in 4% paraformaldehyde (PFA) overnight. After being decalcified with 10% EDTA for 2-4 weeks, the samples were dehydrated in an ethanol and xylene series. Then the samples were embedded in paraffin and cut into 5 μm sections using a microtome (Leica). H&E staining was performed according to standard protocols.

Immunofluorescence

The decalcified samples were dehydrated in serial sucrose solutions, then embedded in optimal cutting temperature compound (Tissue-Tek). The samples were cut into 8 μm cryosections using a cryostat (Leica CM1850). The cryosections were treated with a blocking solution (PerkinElmer) for 1 h. The primary antibodies used were the following: β galactosidase (β-gal) (1:100, Abcam, ab9361, RRID:AB_307210), Periostin (1:100, Abcam, ab14041, RRID:AB_2299859), K14 (1:200, Abcam, ab181595, RRID:AB_2811031)and Ki67 (1:100, Abcam, ab15580, RRID:AB_443209). After being incubated with primary antibodies at 4°C overnight, signals were detected with Alexa-

conjugated secondary antibody (1:200, Invitrogen), and nuclei were stained with DAPI (Invitrogen, 62248). Images were captured with a Keyence microscope (Carl Zeiss).

TUNEL assays

A TUNEL assay kit (Click-iT™ Plus TUNEL Assay for In Situ Apoptosis Detection, Thermo Fisher Scientific, C10617) was used to detect cell apoptosis according to the manufacturer's protocol.

RNA sequencing

After tamoxifen induction, first mandibular molars from the control and *Gli1-Cre^{ER};Fgfr2$^{fl/fl}$* mice were dissected at PN7.5. The apical region of the first molar was collected, and RNA was extracted using a RNeasy Micro Kit (Qiagen, 74004). For RNA-sequencing analysis, cDNA library preparation and sequencing were performed on NextSeq500 High Output equipment for three pairs at the Technology Center for Genomics & Bioinformatics at the University of California, Los Angeles (UCLA), USA. Raw reads were trimmed, aligned with the mm10 genome, and then normalized using upper quartile in Partek Flow. Differential analysis was estimated by selecting transcripts with a significance of $p < 0.05$.

Statistical analysis

Statistical analysis was performed with GraphPad Prism. All statistical data are presented as individual points and mean±SD. Unpaired Student's t-test or one-way ANOVA analysis were used for comparisons, with $p < 0.05$ considered statistically significant. $N \geq 3$ for all experiments.

Acknowledgements

We acknowledge Dr. Bridget Samuels for critical editing of the manuscript, USC Libraries Bioinformatics Service for assisting with data analysis, and the USC Office of Research and the USC Libraries for supporting our access to bioinformatics software and computing resources. This study was supported by funding from the National Institute of Dental and Craniofacial Research, National Institutes of Health (R01 DE022503 and R01 DE012711 to Yang Chai).

Author contributions

F.P. and Y.C. designed the study. F.P., L.M., J.J., Q.W., T.G., M.Z., J.L. and J.H. carried out most of the experiments and data analyses. J.F., E.J., and J.C. provided critical comments. T-V.H. participated in the microCT analysis. F.P. and Y.C. co-wrote the paper. Y.C. supervised the research.

Declaration of conflict of interest

The authors declare that there is no conflict of interest.

Data availability

Bulk RNA-seq datasets and single cell RNA-sequencing (scRNA-Seq) are available through the GEO database under accession code GSE224471 (token: etqtcwogjvyddef).

References:

1. Adameyko, I., and Fried, K. (2016) The Nervous System Orchestrates and Integrates Craniofacial Development: A Review. *Front Physiol* **7**, 49
2. Nedvetsky, P. I., Emmerson, E., Finley, J. K., Ettinger, A., Cruz-Pacheco, N., Prochazka, J., Haddox, C. L., Northrup, E., Hodges, C., Mostov, K. E., Hoffman, M. P., and Knox, S. M. (2014) Parasympathetic innervation regulates tubulogenesis in the developing salivary gland. *Dev Cell* **30**, 449-462
3. Tower, R. J., Li, Z., Cheng, Y. H., Wang, X. W., Rajbhandari, L., Zhang, Q., Negri, S., Uytingco, C. R., Venkatesan, A., Zhou, F. Q., Cahan, P., James, A. W., and Clemens, T. L. (2021) Spatial transcriptomics reveals a role for sensory nerves in preserving cranial suture patency through modulation of BMP/TGF-beta signaling. *Proc Natl Acad Sci U S A* **118**
4. Rizos, M., Negron, R. J., and Serman, N. (1998) Mobius syndrome with dental involvement: a case report and literature review. *Cleft Palate Craniofac J* **35**, 262-268
5. Ruge-Pena, N. O., Valencia, C., Cabrera, D., Aguirre, D. C., and Lopera, F. (2020) Moebius syndrome: Craniofacial clinical manifestations and their association with prenatal exposure to misoprostol. *Laryngoscope Investig Otolaryngol* **5**, 727-733
6. Gao, L., Guo, H., Ye, N., Bai, Y., Liu, X., Yu, P., Xue, Y., Ma, S., Wei, K., Jin, Y., Wen, L., and Xuan, K. (2013) Oral and craniofacial manifestations and two novel missense mutations of the NTRK1 gene identified in the patient with congenital insensitivity to pain with anhidrosis. *PLoS One* **8**, e66863
7. Zhao, H., Feng, J., Seidel, K., Shi, S., Klein, O., Sharpe, P., and Chai, Y. (2014) Secretion of shh by a neurovascular bundle niche supports mesenchymal stem cell homeostasis in the adult mouse incisor. *Cell Stem Cell* **14**, 160-173
8. Pei, F., Ma, L., Jing, J., Feng, J., Yuan, Y., Guo, T., Han, X., Ho, T. V., Lei, J., He, J., Zhang, M., Chen, J. F., and Chai, Y. (2023) Sensory nerve niche regulates mesenchymal stem cell homeostasis via FGF/mTOR/autophagy axis. *Nat Commun* **14**, 344
9. Meyers, C. A., Lee, S., Sono, T., Xu, J., Negri, S., Tian, Y., Wang, Y., Li, Z., Miller, S., Chang, L., Gao, Y., Minichiello, L., Clemens, T. L., and James, A. W. (2020) A Neurotrophic Mechanism Directs Sensory Nerve Transit in Cranial Bone. *Cell Rep* **31**, 107696
10. Jones, R. E., Salhotra, A., Robertson, K. S., Ransom, R. C., Foster, D. S., Shah, H. N., Quarto, N., Wan, D. C., and Longaker, M. T. (2019) Skeletal Stem Cell-Schwann Cell Circuitry in Mandibular Repair. *Cell Rep* **28**, 2757-2766 e2755
11. Scadden, D. T. (2006) The stem-cell niche as an entity of action. *Nature* **441**, 1075-1079
12. van der Kooy, D., and Weiss, S. (2000) Why stem cells? *Science* **287**, 1439-1441
13. Yuan, Y., Loh, Y. H. E., Han, X., Feng, J. F., Ho, T. V., He, J. Z., Jing, J. J., Groff, K., Wu, A., and Chai, Y. (2020) Spatiotemporal cellular movement and fate decisions during first pharyngeal arch morphogenesis. *Sci Adv* **6**
14. Hinck, L. (2004) The versatile roles of "axon guidance" cues in tissue morphogenesis. *Dev Cell* **7**, 783-793
15. May, A. J., Mattingly, A. J., Gaylord, E. A., Griffin, N., Sudiwala, S., Cruz-Pacheco, N., Emmerson, E., Mohabbat, S., Nathan, S., Sinada, H., Lombaert, I. M. A., and Knox, S. M. (2022) Neuronal-epithelial cross-talk drives acinar specification via NRG1-ERBB3-mTORC2 signaling. *Dev Cell* **57**, 2550-2565 e2555
16. Feng, J. F., Jing, J. J., Li, J. Y., Zhao, H., Punj, V., Zhang, T. W., Xu, J., and Chai, Y. (2017) BMP signaling orchestrates a transcriptional network to control the fate of mesenchymal stem cells in mice. *Development* **144**, 2560-2569
17. Li, J. Y., Parada, C., and Chai, Y. (2017) Cellular and molecular mechanisms of tooth root development. *Development* **144**, 374-384

18. Krivanek, J., Adameyko, I., and Fried, K. (2017) Heterogeneity and Developmental Connections between Cell Types Inhabiting Teeth. *Front Physiol* **8**
19. Jing, J. J., Feng, J. F., Yuan, Y., Guo, T. W., Lei, J., Pei, F., Ho, T. V., and Chai, Y. (2022) Spatiotemporal single-cell regulatory atlas reveals neural crest lineage diversification and cellular function during tooth morphogenesis. *Nature Communications* **13**
20. Tummers, M., and Thesleff, I. (2003) Root or crown: a developmental choice orchestrated by the differential regulation of the epithelial stem cell niche in the tooth of two rodent species. *Development* **130**, 1049-1057
21. Hildebrand, C., Fried, K., Tuisku, F., and Johansson, C. S. (1995) Teeth and tooth nerves. *Prog Neurobiol* **45**, 165-222
22. Yokohama-Tamaki, T., Ohshima, H., Fujiwara, N., Takada, Y., Ichimori, Y., Wakisaka, S., Ohuchi, H., and Harada, H. (2006) Cessation of Fgf10 signaling, resulting in a defective dental epithelial stem cell compartment, leads to the transition from crown to root formation. *Development* **133**, 1359-1366
23. Lu, B. C., Cebrian, C., Chi, X., Kuure, S., Kuo, R., Bates, C. M., Arber, S., Hassell, J., MacNeil, L., Hoshi, M., Jain, S., Asai, N., Takahashi, M., Schmidt-Ott, K. M., Barasch, J., D'Agati, V., and Costantini, F. (2009) Etv4 and Etv5 are required downstream of GDNF and Ret for kidney branching morphogenesis. *Nat Genet* **41**, 1295-1302
24. Herriges, J. C., Verheyden, J. M., Zhang, Z., Sui, P., Zhang, Y., Anderson, M. J., Swing, D. A., Zhang, Y., Lewandoski, M., and Sun, X. (2015) FGF-Regulated ETV Transcription Factors Control FGF-SHH Feedback Loop in Lung Branching. *Dev Cell* **35**, 322-332
25. Zhang, Z., Verheyden, J. M., Hassell, J. A., and Sun, X. (2009) FGF-regulated Etv genes are essential for repressing Shh expression in mouse limb buds. *Dev Cell* **16**, 607-613
26. Sigafoos, A. N., Paradise, B. D., and Fernandez-Zapico, M. E. (2021) Hedgehog/GLI Signaling Pathway: Transduction, Regulation, and Implications for Disease. *Cancers (Basel)* **13**
27. Carballo, G. B., Honorato, J. R., de Lopes, G. P. F., and Spohr, T. (2018) A highlight on Sonic hedgehog pathway. *Cell Commun Signal* **16**, 11
28. Liu, Y., Feng, J., Li, J., Zhao, H., Ho, T. V., and Chai, Y. (2015) An Nfic-hedgehog signaling cascade regulates tooth root development. *Development* **142**, 3374-3382
29. Jeong, J., Mao, J., Tenzen, T., Kottmann, A. H., and McMahon, A. P. (2004) Hedgehog signaling in the neural crest cells regulates the patterning and growth of facial primordia. *Genes Dev* **18**, 937-951
30. Bai, C. B., Auerbach, W., Lee, J. S., Stephen, D., and Joyner, A. L. (2002) Gli2, but not Gli1, is required for initial Shh signaling and ectopic activation of the Shh pathway. *Development* **129**, 4753-4761
31. Ahn, S., and Joyner, A. L. (2004) Dynamic changes in the response of cells to positive hedgehog signaling during mouse limb patterning. *Cell* **118**, 505-516
32. Molotkov, A., Mazot, P., Brewer, J. R., Cinalli, R. M., and Soriano, P. (2017) Distinct Requirements for FGFR1 and FGFR2 in Primitive Endoderm Development and Exit from Pluripotency. *Dev Cell* **41**, 511-526.e514
33. Xie, W., Chow, L. T., Paterson, A. J., Chin, E., and Kudlow, J. E. (1999) Conditional expression of the ErbB2 oncogene elicits reversible hyperplasia in stratified epithelia and up-regulation of TGFalpha expression in transgenic mice. *Oncogene* **18**, 3593-3607
34. Perl, A. K., Wert, S. E., Nagy, A., Lobe, C. G., and Whitsett, J. A. (2002) Early restriction of peripheral and proximal cell lineages during formation of the lung. *Proc Natl Acad Sci U S A* **99**, 10482-10487
35. Hao, Y., Hao, S., Andersen-Nissen, E., Mauck, W. M., 3rd, Zheng, S., Butler, A., Lee, M. J., Wilk, A. J., Darby, C., Zager, M., Hoffman, P., Stoeckius, M., Papalexi, E., Mimitou, E. P., Jain, J., Srivastava, A., Stuart, T., Fleming, L. M., Yeung, B., Rogers, A. J., McElrath, J. M., Blish, C. A., Gottardo, R.,

Smibert, P., and Satija, R. (2021) Integrated analysis of multimodal single-cell data. *Cell* **184**, 3573-3587 e3529

36. Guerrero-Juarez, C. F., Dedhia, P. H., Jin, S., Ruiz-Vega, R., Ma, D., Liu, Y., Yamaga, K., Shestova, O., Gay, D. L., Yang, Z., Kessenbrock, K., Nie, Q., Pear, W. S., Cotsarelis, G., and Plikus, M. V. (2019) Single-cell analysis reveals fibroblast heterogeneity and myeloid-derived adipocyte progenitors in murine skin wounds. *Nat Commun* **10**, 650

Figure Legends

Fig. 1: Sensory nerve regulates cells in molar through FGF signaling at the initiation of tooth root development. (A) Schematic drawing of molar at PN3.5 with relevant cell populations labeled. (B-D) Distribution of nerves in the first molar. White arrows indicate nerve fibers in coronal papilla; yellow arrows indicate that nerve fibers enter from apical papilla. White dotted line indicates the outline of the papilla in the molar. (E) UMAP visualization of clusters from the trigeminal ganglion at PN3.5. SN1-3, sensory neuron types 1-3; SC, Schwann cell; SMA, arterial smooth muscle. (F) Significant signals derived from sensory nerve interact with the first molar at the initiating stage of tooth root development. Bar plots on the top represent the total outgoing/incoming interaction scores and the right represents the outgoing/incoming signal strength of each signaling pathway. TG, neural progenitors and sensory neurons in trigeminal ganglion; PA, papilla cells; FO, follicle cells; EP, epithelial cells; PA, FO, EP are clusters in molar. Red box highlights FGF signaling. (G) Hierarchical plot shows the inferred FGF signaling intercellular communication network. Circle sizes indicate the number of cells in each cluster; bigger circle size means more cells in the cluster. TG, neural progenitors and sensory neurons in trigeminal ganglion; PA, papilla cells; FO, follicle cells; EP, epithelium cells; PA, FO, EP are clusters in molar. (H) Expression of *Fgf1* for cell clusters in the mouse trigeminal ganglion. (I-J) The expression of neurofilament and *Fgf1* in the trigeminal ganglion at PN3.5. (K) Feature plot of *Fgf1* in different clusters in the mouse molar. (L-M) The expression of *Fgf1* in the first molar at P3.5. (N-P) The protein level of FGF1 in the first molar at P3.5. Scale bars, 100 μm.

Fig. 2: *Fgfr2* is expressed in *Gli1*$^{+}$ progenitor cells during tooth root development. (A) 16 clusters from the first molar at PN3.5 on a UMAP visualization. (B) Feature plot of *Fgfr2* and *Gli1* in molar clusters. (C-D) Expression of *Fgfr2* and *Gli1*$^{+}$ cells stained with β-gal in molar from *Gli1-LacZ* mouse. White arrows indicate the colocalization of *Fgfr2* and β-gal. (E-J) Expression of *Fgfr2* in mandibular first molar from wild-type mice at PN3.5, PN13.5 and PN21.5. White arrows point to the expression of *Fgfr2* in follicle cells; yellow arrows point to the expression of *Fgfr2* in apical papilla cells; white arrowheads point to the expression of *Fgfr2* in periodontal tissue. White dashed lines outline Hertwig's epithelial root sheath (HERS). Scale bars, 100 μm.

Fig. 3: Loss of *Fgfr2* in *Gli1*$^{+}$ progenitor cells leads to short roots with impaired proliferation and differentiation. (A-D) MicroCT analysis of the first mandibular molars in *Fgfr2*$^{fl/fl}$ and *Gli1-Cre*^{ER}*;Fgfr2*$^{fl/fl}$ mice at PN21.5. Line with arrows indicates the root length. (E) Quantification of root length in control and mutant mice. P=0.0007. (F-G) Histological analysis of *Fgfr2*$^{fl/fl}$ and *Gli1-Cre*^{ER}*;Fgfr2*$^{fl/fl}$ mice. (H-I) *Dspp* expression in *Fgfr2*$^{fl/fl}$ and *Gli1-Cre*^{ER}*;Fgfr2*$^{fl/fl}$ mice. White and yellow arrows point to the expression of *Dspp* in root and furcation respectively; white and yellow arrowheads point to the defective odontoblast differentiation in mutant mice. (J-K) Periostin expression in *Fgfr2*$^{fl/fl}$ and *Gli1-Cre*^{ER}*;Fgfr2*$^{fl/fl}$ mice. White and yellow arrows point to the expression of periostin in periodontal ligament of lateral and furcation regions; white and yellow arrowheads point to the defective periodontal ligament differentiation in mutant mice. (L) Relative fluorescent intensity of *Dspp.* P=0.0014. (M) Relative fluorescent intensity of periostin. P<0.0001. (N-Q) Proliferating cells stained with Ki67 in *Fgfr2*$^{fl/fl}$ and *Gli1-Cre*^{ER}*;Fgfr2*$^{fl/fl}$ mice at PN7.5. (R) Quantification of Ki67^{+} cells in control and mutant mice. Unpaired

Student's t-test, P<0.0001. n = 3. Each data point represents one animal. All data are expressed as the mean ± SD. Source data are provided as a Source Data file. White dashed lines outline HERS. Schematic at the bottom indicates induction protocol. Scale bars, A-D, 1mm; N-Q, 100 μm; others, 500 μm.

Fig. 4: Loss of FGF signaling in tooth root mesenchymal progenitors leads to compromised Hh signaling. (A) Hierarchical clustering showing the gene expression profiles of control and *Gli1-Cre^{ER};Fgfr2$^{fl/fl}$* mice. (B) Volcano plot showing 413 upregulated genes and 326 downregulated genes in mutant relative to control. (C) GO analysis shows the signaling pathways involved. (D-G) Expression of *Ptch1* in *Fgfr2$^{fl/fl}$* and *Gli1-Cre^{ER};Fgfr2$^{fl/fl}$* mice at PN7.5. White arrows point to the expression of *Ptch1* in dental papilla; white arrowheads point to the expression in dental follicle; white asterisk indicates the expression in dental epithelium. (H) Relative fluorescent intensity of *Ptch1.* P=0.002. (I-L) Expression of *Gli1* in *Fgfr2$^{fl/fl}$* and *Gli1-Cre^{ER};Fgfr2$^{fl/fl}$* mice at PN7.5. White arrows point to the expression of *Gli1* in dental papilla; white arrowheads point to the expression in dental follicle; white asterisk indicates the expression in dental epithelium. (M) Relative fluorescent intensity of *Gli1.* Unpaired Student's t-test, P=0.0007. N = 3. Each data point represents one animal. All data are expressed as the mean ± SD. Source data are provided as a Source Data file. White dashed lines outline HERS. Scale bars, 100 μm.

Fig. 5: Impaired SHH leads to decreased Hh signaling in *Gli1-Cre^{ER};Fgfr2$^{fl/fl}$* mice. (A) Different cell clusters in the mandibular first molar at PN3.5. (B) Feature plot of Hh ligands in different clusters in the mandibular first molar at PN3.5. (C-E) Expression of *Shh, Dhh* and *Ihh* in first molar at PN3.5. White dashed box indicates higher magnification of apical epithelium. (F) Plot of *Shh* with RNAseq in control and mutant mice shows

decreased expression of *Shh*. (G-J) Expression of *Shh* in *Fgfr2*$^{fl/fl}$ and *Gli1-Cre*^{ER}*;Fgfr2*$^{fl/fl}$ mice at PN7.5. (K-N) Protein levels of SHH in *Fgfr2*$^{fl/fl}$ and *Gli1-Cre*^{ER}*;Fgfr2*$^{fl/fl}$ mice at PN7.5. (O) Relative fluorescent intensity of *Shh* in control (H) and mutant (J) mice. Unpaired Student's t-test, P<0.0001. N = 3. Each data point represents one animal. All data are expressed as the mean ± SD. Source data are provided as a Source Data file. White dashed lines outline HERS. Schematic at the bottom indicates induction protocol. Scale bars, 100 μm.

Fig. 6: Activation of Hh signaling partially restores root defects in *Gli1-Cre*^{ER}*;Fgfr2*$^{fl/fl}$ mice. (A-F) MicroCT analysis of the first mandibular molars in *Fgfr2*$^{fl/fl}$, *Gli1-Cre*^{ER}*;Fgfr2*$^{fl/fl}$ and *Gli1-Cre*^{ER}*;Fgfr2*$^{fl/fl}$;*SmoM2*$^{fl/+}$ mice at PN21.5. Lines with arrows indicate the root length. (G) Quantification of root length in the three groups. *Fgfr2*$^{fl/fl}$ versus *Gli1-Cre*^{ER}*;Fgfr2*$^{fl/fl}$: P=0.0011; *Gli1-Cre*^{ER}*;Fgfr2*$^{fl/fl}$ versus *Gli1-Cre*^{ER}*;Fgfr2*$^{fl/fl}$;*SmoM2*$^{fl/+}$: P=0.0169. (H-J) Histological analysis of *Fgfr2*$^{fl/fl}$, *Gli1-Cre*^{ER}*;Fgfr2*$^{fl/fl}$ and *Gli1-Cre*^{ER}*;Fgfr2*$^{fl/fl}$;*SmoM2*$^{fl/+}$ mice. (K-M) *Dspp* and periostin expression in *Fgfr2*$^{fl/fl}$, *Gli1-Cre*^{ER}*;Fgfr2*$^{fl/fl}$ and *Gli1-Cre*^{ER}*;Fgfr2*$^{fl/fl}$;*SmoM2*$^{fl/+}$ mice. White arrows point to the expression of *Dspp* and periostin in root and furcation; white arrowheads point to the abnormal *Dspp* and periostin expression in mutant mice. (N) Relative fluorescent intensity of *Dspp. Fgfr2*$^{fl/fl}$ versus *Gli1-Cre*^{ER}*;Fgfr2*$^{fl/fl}$: P<0.0011; *Gli1-Cre*^{ER}*;Fgfr2*$^{fl/fl}$ versus *Gli1-Cre*^{ER}*;Fgfr2*$^{fl/fl}$;*SmoM2*$^{fl/+}$: P=0.0001. (O) Relative fluorescent intensity of periostin. *Fgfr2*$^{fl/fl}$ versus *Gli1-Cre*^{ER}*;Fgfr2*$^{fl/fl}$: P<0.0011; *Gli1-Cre*^{ER}*;Fgfr2*$^{fl/fl}$ versus *Gli1-Cre*^{ER}*;Fgfr2*$^{fl/fl}$;*SmoM2*$^{fl/+}$: P<0.0001. (P-U) Proliferating cells stained with Ki67 in *Fgfr2*$^{fl/fl}$, *Gli1-Cre*^{ER}*;Fgfr2*$^{fl/fl}$ and *Gli1-Cre*^{ER}*;Fgfr2*$^{fl/fl}$;*SmoM2*$^{fl/+}$ mice at PN7.5. (V) Quantification of Ki67^{+} cells in the three groups. *Fgfr2*$^{fl/fl}$ versus *Gli1-Cre*^{ER}*;Fgfr2*$^{fl/fl}$:

P<0.0011; *Gli1-Cre*^{ER};*Fgfr2*$^{fl/fl}$ versus *Gli1-Cre*^{ER};*Fgfr2*$^{fl/fl}$;*SmoM2*$^{fl/+}$: P<0.0001. N = 3. Each data point represents one animal. All data are expressed as the mean ± SD and groups were compared with one-way ANOVA. Source data are provided as a Source Data file. White dashed lines outline HERS. Schematic at the bottom indicates induction protocol. Scale bars, A-F, 1mm; P-U, 100 μm; others, 500 μm.

Fig. 7: Schematic of sensory nerve regulation of progenitor cells via FGF-SHH-Hh axis during tooth root development. Sensory nerves are enriched in the molar at the initiation of tooth root development. FGFR2 is expressed in *Gli1*$^{+}$ progenitors in the molar. Sensory nerve-derived FGF signaling regulates *Gli1*$^{+}$ progenitors to modulate tooth root development through FGFR2. Loss of *Fgfr2* in *Gli1*$^{+}$ progenitors leads to decreased proliferation alongside impaired differentiation. *Shh* is downregulated in the epithelium after loss of FGF signaling and leads to impaired Hh signaling in both epithelium and mesenchyme, which in turn decreases proliferation and differentiation in mutant mice. Schematic was created with BioRender.

Figure 1

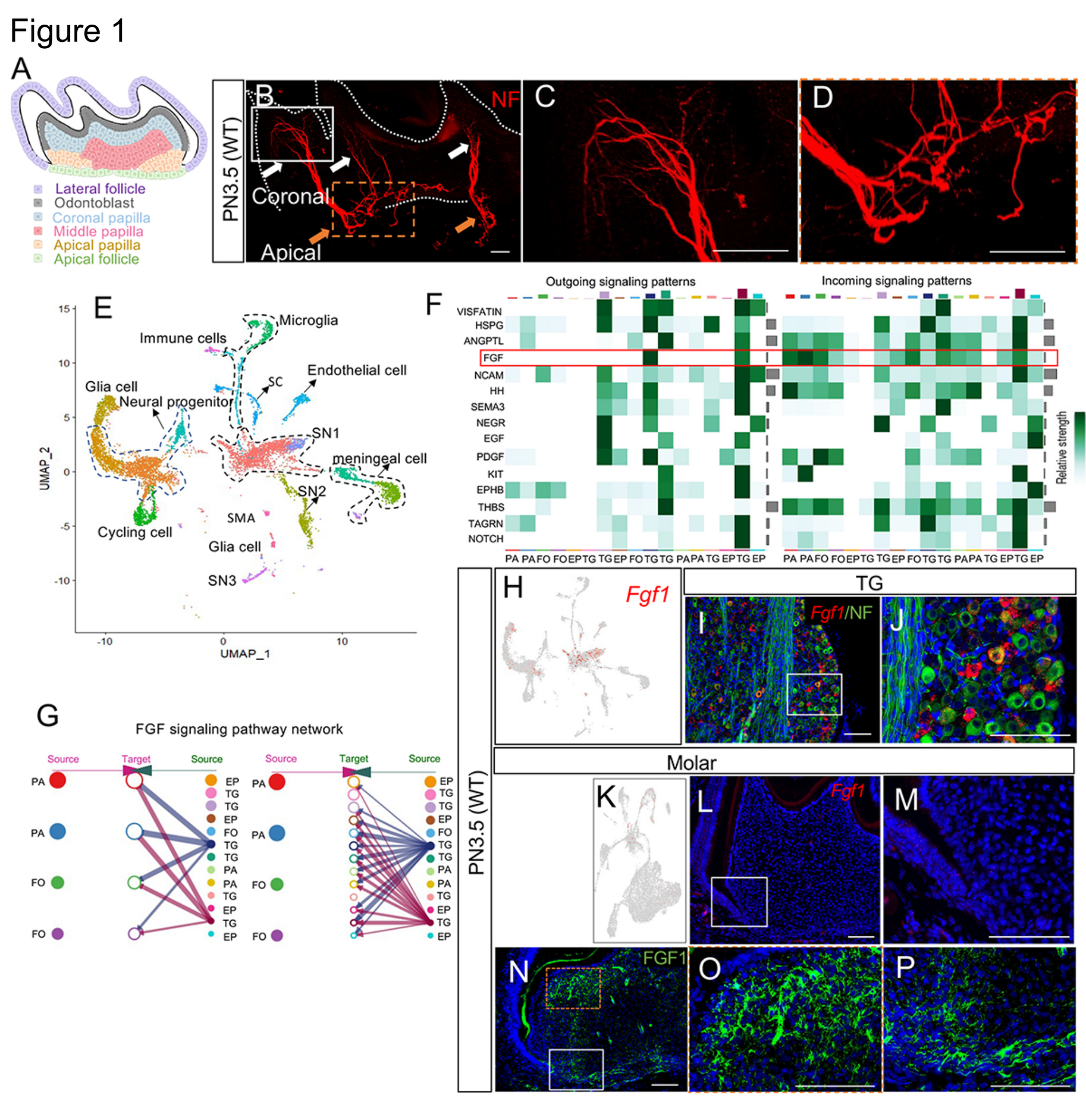
A
Lateral follicle
Odontoblast
Coronal papilla
Middle papilla
Apical papilla
Apical follicle
PN3.5 (WT)
B
NF
Coronal
Apical
C
D
E
Microglia
Immune cells
Endothelial cell
SC
Glia cell
Neural progenitor
SN1
meningeal cell
SN2
SMA
Cycling cell
Glia cell
SN3
UMAP_1
UMAP_2
F
Outgoing signaling patterns
Incoming signaling patterns
VISFATIN
HSPG
ANGPTL
FGF
NCAM
HH
SEMA3
NEGR
EGF
PDGF
KIT
EPHB
THBS
TAGRN
NOTCH
Relative strength
G
FGF signaling pathway network
Source
Target
Source
H
Fgf1
TG
I
Fgf1/NF
J
Molar
K
L
Fgf1
M
N
FGF1
O
P

Figure 2

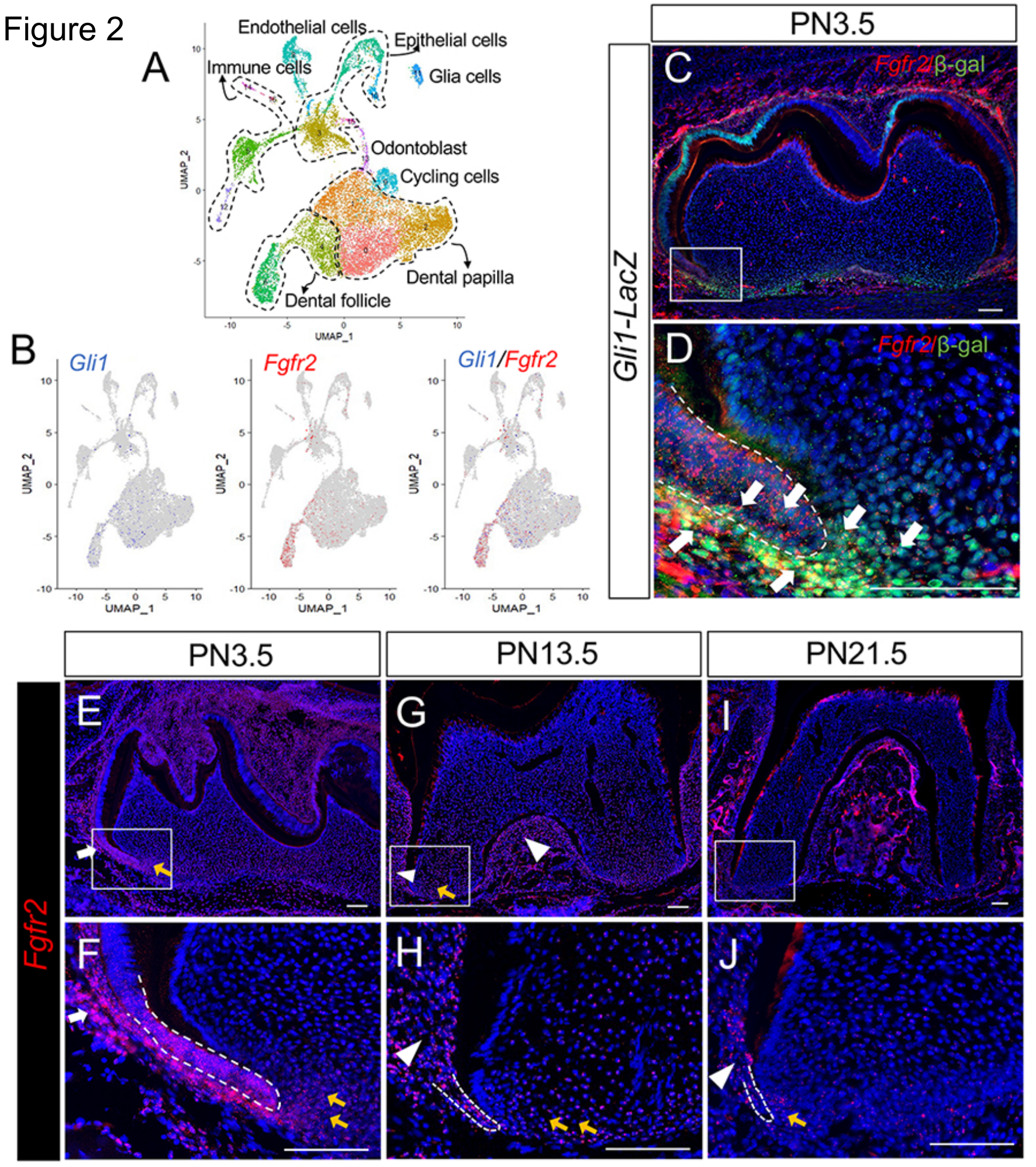
A
Endothelial cells
Epithelial cells
Immune cells
Glia cells
Odontoblast
Cycling cells
Dental papilla
Dental follicle
UMAP_1
UMAP_2
B
Gli1
Fgfr2
Gli1/Fgfr2
PN3.5
Gli1-LacZ
C
Fgfr2/β-gal
D
Fgfr2/β-gal
PN3.5
PN13.5
PN21.5
Fgfr2
E
F
G
H
I
J

Figure 3

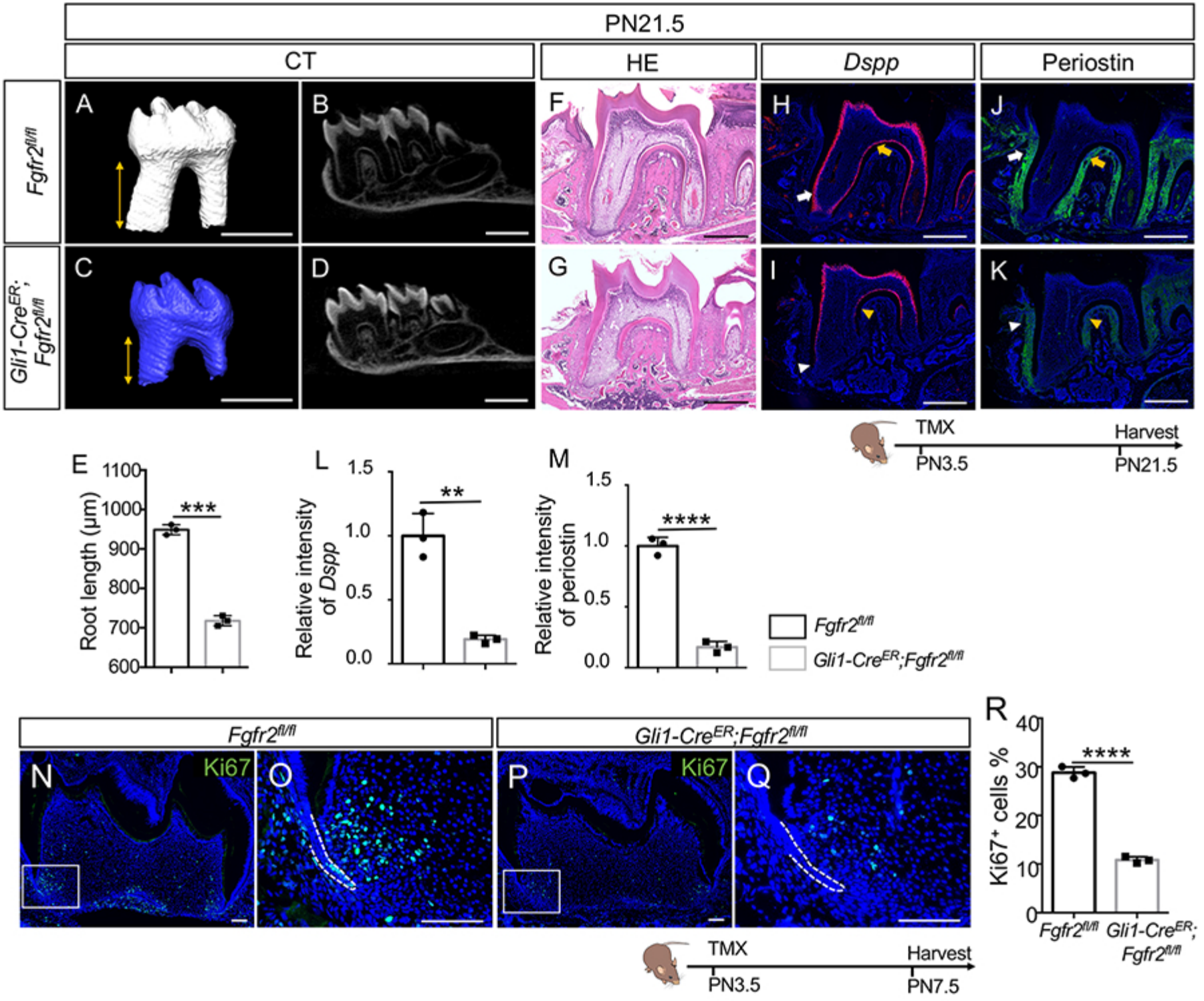
PN21.5
CT
HE
Dspp
Periostin
Fgfr2fl/fl
Gli1-CreER; Fgfr2fl/fl
A
B
C
D
F
G
H
I
J
K
TMX
PN3.5
Harvest
PN21.5
E
Root length (μm)
1100
1000
900
800
700
600
***
L
Relative intensity of Dspp
1.5
1.0
0.5
0.0
**
M
Relative intensity of periostin
1.5
1.0
0.5
0.0
****
Fgfr2fl/fl
Gli1-CreER;Fgfr2fl/fl
Fgfr2fl/fl
Gli1-CreER;Fgfr2fl/fl
N
Ki67
O
P
Ki67
Q
TMX
PN3.5
Harvest
PN7.5
R
Ki67+ cells %
40
30
20
10
0
****
Fgfr2fl/fl
Gli1-CreER; Fgfr2fl/fl

Figure 4

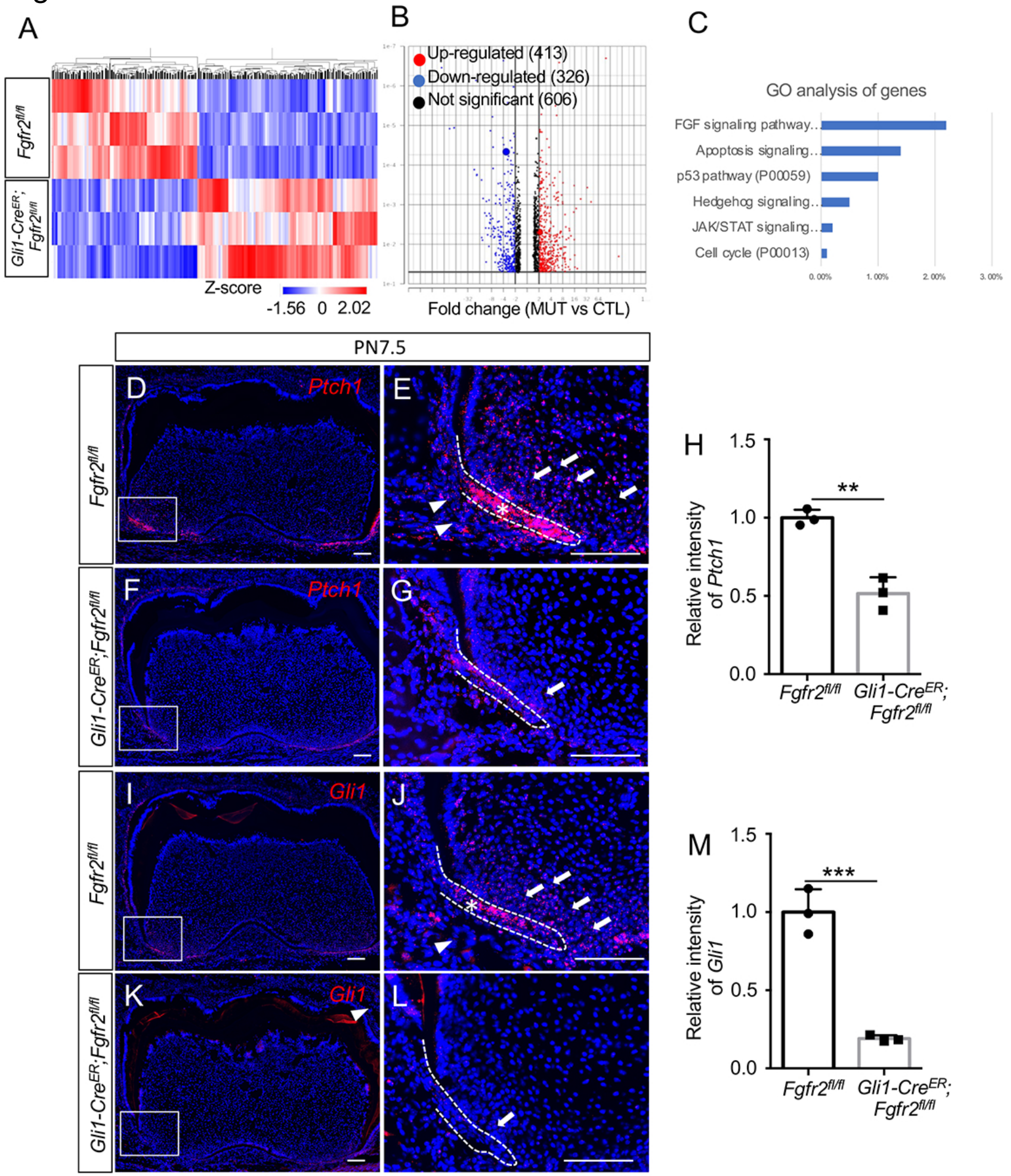
A
Fgfr2fl/fl
Gli1-CreER; Fgfr2fl/fl
Z-score
-1.56 0 2.02
B
Up-regulated (413)
Down-regulated (326)
Not significant (606)
Fold change (MUT vs CTL)
C
GO analysis of genes
FGF signaling pathway...
Apoptosis signaling...
p53 pathway (P00059)
Hedgehog signaling...
JAK/STAT signaling...
Cell cycle (P00013)
0.00%
1.00%
2.00%
3.00%
PN7.5
D
Ptch1
E
F
Ptch1
G
Gli1-CreER;Fgfr2fl/fl
I
Gli1
J
K
Gli1
L
H
Relative intensity of Ptch1
1.5
1.0
0.5
0.0
**
Fgfr2fl/fl
Gli1-CreER; Fgfr2fl/fl
M
Relative intensity of Gli1
1.5
1.0
0.5
0.0
***
Fgfr2fl/fl
Gli1-CreER; Fgfr2fl/fl

Figure 5

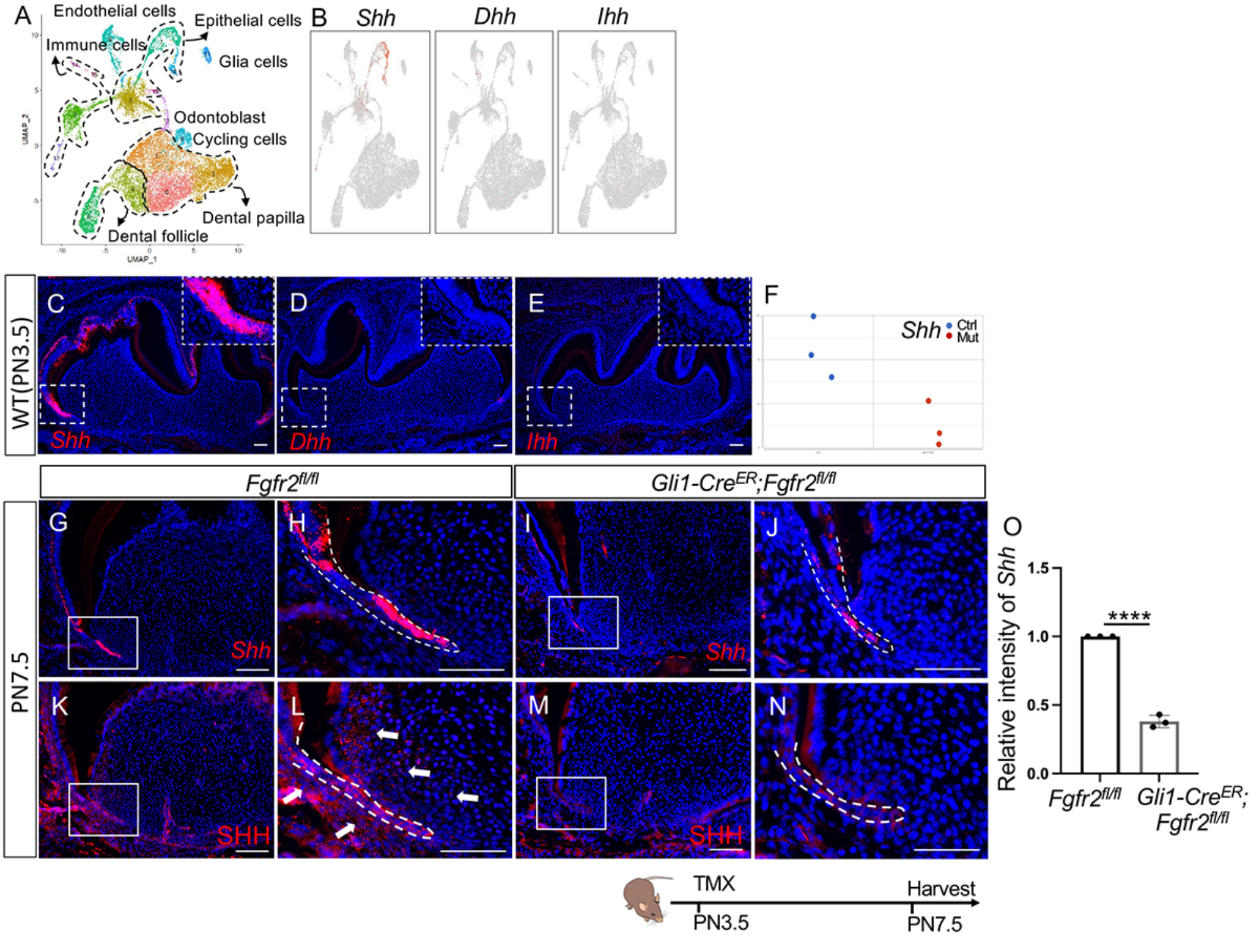
A
Endothelial cells
Epithelial cells
Immune cells
Glia cells
Odontoblast
Cycling cells
Dental papilla
Dental follicle
UMAP_1
UMAP_2
B
Shh
Dhh
Ihh
WT(PN3.5)
C
D
E
Shh
Dhh
Ihh
F
Shh
Ctrl
Mut
Fgfr2fl/fl
Gli1-CreER;Fgfr2fl/fl
PN7.5
G
H
I
J
K
L
M
N
Shh
SHH
O
Relative intensity of Shh
1.5
1.0
0.5
0.0
****
Fgfr2fl/fl
Gli1-CreER; Fgfr2fl/fl
TMX
PN3.5
Harvest
PN7.5

Figure 6

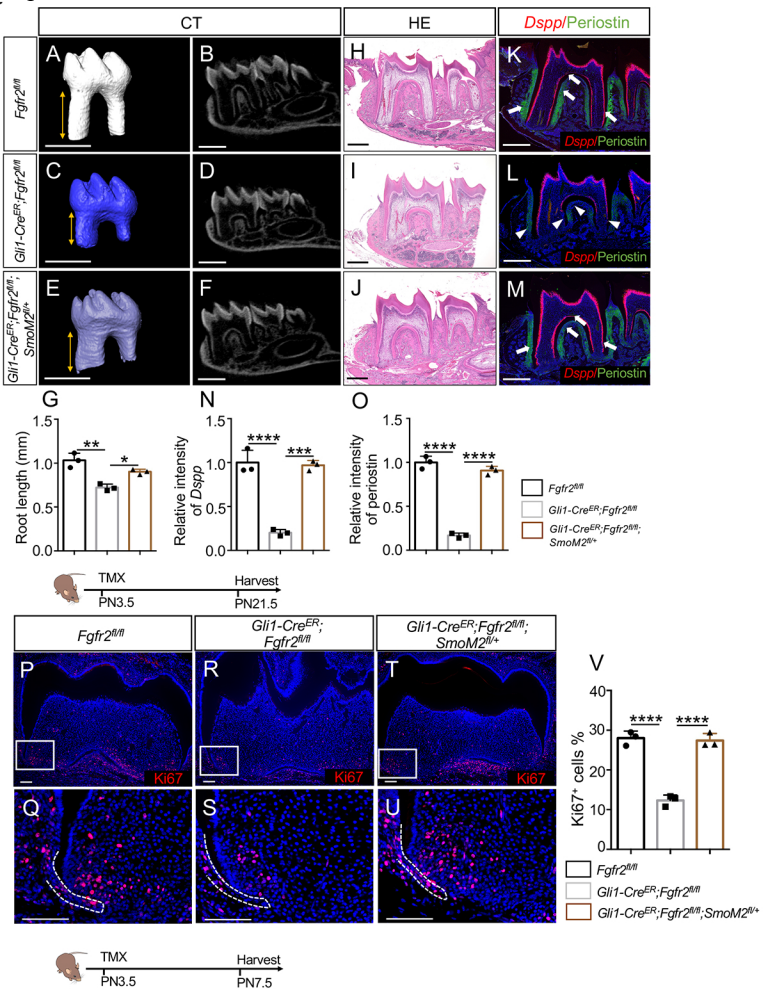
CT
HE
Dspp/Periostin
Fgfr2fl/fl
Gli1-CreER;Fgfr2fl/fl
Gli1-CreER;Fgfr2fl/fl; SmoM2fl/+
A
B
C
D
E
F
H
I
J
K
L
M
Dspp/Periostin
G
N
O
Root length (mm)
Relative intensity of Dspp
Relative intensity of periostin
1.5
1.0
0.5
0.0
**
*
****
***
****
****
Fgfr2fl/fl
Gli1-CreER;Fgfr2fl/fl
Gli1-CreER;Fgfr2fl/fl; SmoM2fl/+
TMX
PN3.5
Harvest
PN21.5
Fgfr2fl/fl
Gli1-CreER; Fgfr2fl/fl
Gli1-CreER;Fgfr2fl/fl; SmoM2fl/+
P
R
T
Q
S
U
Ki67
V
Ki67+ cells %
40
30
20
10
0
****
****
Fgfr2fl/fl
Gli1-CreER;Fgfr2fl/fl
Gli1-CreER;Fgfr2fl/fl;SmoM2fl/+
TMX
PN3.5
Harvest
PN7.5

Figure 7

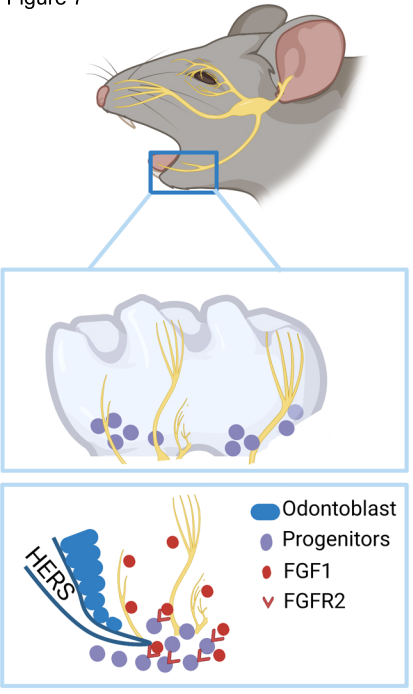
Control
Differentiation
Proliferation
Epithelial cells
Gli1+ progenitor cells
Fgfr2-KO
FGF signaling
Hedgehog signaling
HH ligand (SHH)
Impaired proliferation and differentiation
HERS
Odontoblast
Progenitors
FGF1
FGFR2